THE JOURNAL OF PHYSICAL CHEMISTRY C

pubs.acs.org/JPCC Article

Probing Conformational Evolution and Associated Dynamics of $Mg(N(SO_2CF_3)_2)_2$·Dimethoxyethane Adduct Using Solid-State ^{19}F and ^1H NMR

Ying Chen, Nicholas R. Jaegers, Kee Sung Han, Hui Wang, Robert P. Young, Garvit Agarwal, Andrew S. Lipton, Rajeev S. Assary, Nancy M. Washton, Jian Zhi Hu, Karl T. Mueller,* and Vijayakumar Murugesan*

Cite This: J. Phys. Chem. C 2020, 124, 4999−5008 Read Online

ACCESS | Metrics & More | Article Recommendations | Supporting Information

ABSTRACT: Bis(trifluoromethanesulfonimide) or TFSI is widely used as a counter anion in electrolyte design due to its structural flexibility and chemical stability. We studied the conformational variations and associated dynamics of TFSI in adduct of $Mg(TFSI)_2$ with dimethoxyethane (DME), a solvate crystalline material using solid-state ^1H and ^{19}F NMR. TFSI molecular motion in this solvate structure falls within the timescale of the ^{19}F NMR experiment, yielding spectroscopic signatures for unique TFSI conformers under the coordination environment of Mg^{2+} cation. Within the temperature range of −5 to 82 °C, we observe nine distinct TFSI sites in both crystalline and disordered regions using ^{19}F NMR, reflecting complexity of structural and dynamics of TFSI anions within solvate structure. The four distinguishable sites in the disordered region for the two CF_3 groups of the same TFSI molecule are identified using chemical shift analysis. The exchange rate constants from site to site are calculated through variable temperature ^{19}F NMR and two-dimensional (2D) exchange spectroscopy (EXSY) experiments, along with respective activation enthalpies using Eyring's formulation. The flip rate of CF_3 around the S−C bond is estimated as ∼15 s^{-1} at 8 °C with $\Delta H^{\neq} \sim 22$ kJ/mol, but the rotation of the entire TFSI is 4.8 s^{-1} at 8 °C with a significantly greater $\Delta H^{\neq} = 98 \pm 10$ kJ/mol. Furthermore, the slow conversion of trans to cis conformers at a lower temperature ($T \leq 1$ °C) in the crystalline region is monitored, with a conversion rate of $\sim 2 \times 10^{-5}$ s^{-1} at −5 °C. Density functional theory (DFT)-based calculations were performed to support further the assignment of experimental chemical shifts, and the activation energy $E_a = 21.1$ kJ/mol obtained for the cis to trans transition is consistent with experimental values. The combined set of ^{19}F and ^1H under both one-dimensional (1D) and 2D NMR methods demonstrated here can be further used for examining electrode−electrolyte interfaces to probe the motions of various constituents that can enable detailed studies of interfacial processes and dynamics. Ultimately, such studies will aid in the design and discovery of interfacial constructs in which directed defect chemistry, chemical moiety distribution, and nanostructure are employed to drive efficient charge transport.

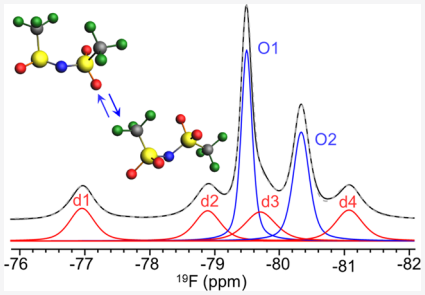

INTRODUCTION

Bis(trifluoromethanesulfonimide) (TFSI) is a weekly coordinating anion widely used in ionic liquid (IL) solvents[1,2] and is gaining greater attention as a promising electrolyte component in next-generation multivalent batteries.[3−6] For example, as the only readily ether-soluble simple Mg salt, $Mg(TFSI)_2$−$Mg(N(SO_2CF_3)_2)_2$—has demonstrated remarkable electrochemical behaviors, such as a wide electrochemical stability window and notable ion conductivity.[6−11] The enhanced solubility and electrochemical properties can be ascribed to the conformational flexibility of TFSI anions along with their extensive delocalized negative charge leading to a particularly weak coordinating power. Both theoretical and experimental studies have supported the existence of two conformers of C1 (cis) and C2 (trans) symmetry in TFSI-containing solutions and solids (Scheme 1),[12,13] with the trans conformer 2−5 kJ/mol more stable in the gas phase, but the cis conformer is

Scheme 1. Cis and Trans Conformers of TFSI[a]

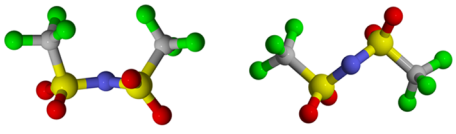

[a]Atom color scheme: carbon = gray, nitrogen = blue, oxygen = red, fluorine = green, and sulfur = yellow.

Received: October 30, 2019
Revised: January 14, 2020
Published: February 7, 2020

preferred for coordinating multivalent metal ions due to its larger dipole moment (μ = 5.42 D for C1 compared with 0.67 D for C2).[12] In addition to the cis and trans conformers, TFSI anions can also establish mono- and bidentate coordinations involving sulfonyl oxygens and cation(s) as part of electrolyte solvation structures. These structural variations are complex and coupled closely to the thermodynamic landscape of ion diffusion pathways and exogenic forces (such as temperature and electric field), and therefore both structure and dynamics can play a critical role in the overall battery performance. For example, the solvate structure evolution near electrode−electrolyte interfaces during de- and resolvation processes of cations in the presence of TFSI anions and solvent molecules will be critical in determining the rate of ion transfer between electrode and electrolyte. However, the absolute determination of the active solvate structure(s) enabling charge transfer remains elusive, necessitating ever more detailed molecular-level investigations of electrolyte constituents.

Typical spectroscopic approaches such as IR and Raman studies exploit the specific vibrational modes of TFSI for analyzing conformational structures and provide specific spectral signatures for the two stable rotamers.[6,12−15] However, the intrinsically weak signal intensity, potential fluorescence effect, and interfering peaks from other species may affect spectral interpretation. X-ray crystallography, especially single-crystal X-ray diffraction (SCXRD), directly detects TFSI geometries and has been used to determine the fraction of each conformer in several TFSI-containing solids, but a well-defined crystal structure is required for the measurements and dynamics information is usually inaccessible.[9,16−20] As one of the most sensitive NMR active nuclei, ^{19}F has proven to be a valuable probe in chemical, biological, and materials studies due to its wide chemical shift range and high sensitivity to its local chemical environment.[21] ^{19}F NMR has been used in several TFSI-containing solutions and ionic liquids providing useful information regarding the ion pairing of TFSI via self-diffusion coefficients measured by ^{19}F pulsed-field gradient (PFG) NMR and about molecular rotational motions via NMR relaxation measurements.[14,22−25] However, only a single ^{19}F NMR resonance is observed due to the fast exchange rates ($\geq\mu$s) between the conformers and associated structural variations within liquid electrolytes. As the solvent and/or anion exchange process within cation solvation structure can lead to motional averaging of NMR signal, NMR spectroscopic signatures and associated dynamics of different TFSI conformers within cation solvate structures can best be obtained if we limit (or "slow down") molecular motion.

Nucleating crystals from saturated TFSI-based salt solution provide adduct structures containing TFSI, cations, and solvent molecules. This crystalline adduct structure represents a possible low-energy solvation structure and offers a unique opportunity to study the conformational flexibility of TFSI in the presence of counter cations and solvent molecules with dampened molecular motions that can readily be probed by NMR. In this work, we first present ^{19}F magic angle spinning (MAS) NMR spectra on three TFSI-containing salts (LiTFSI, NaTFSI, and $Mg(TFSI)_2$), which show a general trend where signal from the cis conformer is shifted downfield from the trans conformer but the broad signals resulting from slow molecular motion in salts prevent detailed structural and dynamic analysis. We then move to an adduct sample, $Mg(TFSI)_2$·DME, where TFSI motion is slower than in pure liquids but faster than in pure salts, thereby enabling a detailed analysis of conformal structure and associated dynamics. ^{19}F single-pulse one-dimensional (1D) and 2D nuclear Overhauser effect spectroscopy (NOESY) and rotating frame Overhauser effect spectroscopy (ROESY) NMR studies of this adduct produce distinguishable signals for TFSI anions located in the ordered (crystalline) or disordered regions, adopting cis or trans conformations. The conformational exchange rates between the conformers at varying temperatures are calculated from these 2D experiments. Additionally, density functional theory (DFT) calculations of ^{19}F chemical shifts and the activation energy of cis to trans isomerization are consistent with the experimental values.

EXPERIMENTAL METHODS

Sample Preparation. Salts of LiTFSI (Battery-grade, BASF), NaTFSI, and $Mg(TFSI)_2$ (99.5%, Solvionic) were dried for 2 days under vacuum at 180 °C prior to usage. The dimethoxyethane (DME) solvent (Battery-grade, Gotion) was further dried over activated 3 Å molecular sieves in a glovebox until its moisture content was determined to be below 30 ppm using a Karl-Fisher Titrator (Metrohm). $Mg(TFSI)_2$ was dried for 2 days under vacuum at 180 °C until just before NMR measurements were made. $Mg(TFSI)_2$·DME crystals were prepared on the basis of a previously reported preparation method:[9] 3.65 g of $Mg(TFSI)_2$ was dissolved and stirred in 4.5 g of DME at 80 °C for 24 h until no solids were visible in this solution. Subsequently, the hot solution was filtered through a 0.45 μm syringe filter and the resulting filtrate was left undisturbed until it reached ambient temperature to separate out crystals.

One-Dimensional ^{1}H and ^{19}F NMR. All samples were packed into 2.5 mm Bruker NMR rotors inside a glovebox with a nitrogen atmosphere immediately before NMR measurement to minimize the influence of moisture. Dry nitrogen gas was used for MAS drive and bearing pressure, thus further protecting the sample from moisture contact. Rotors allowed to remain at ambient laboratory atmosphere for even a few hours between measurements produced slightly different spectra; therefore, a fresh sample was prepared for each measurement. All experiments were repeated three times with freshly packed rotors. ^{1}H and ^{19}F magic angle spinning (MAS) NMR spectra were collected on a Bruker Avance III spectrometer with a field strength of 600 MHz (14.1 T) at a spinning speed of 24 kHz. The 90° pulse width was 3.2 μs for ^{1}H, and 3.3 μs, for ^{19}F. The ^{1}H and ^{19}F spectra were obtained using single-pulse excitation with 32 scans and a recycle delay of 20 s for quantitative comparison. For variable temperature MAS measurements (from −5 to 82 °C), temperature calibrations were performed at various spinning speeds using lead nitrate ($Pb(NO_3)_2$) powder as the sample temperature within a spinning rotor can be significantly different from the probe set temperature (Supporting Information).[26,27] In variable temperature experiments, a series of spectra were measured once the temperature reading became stable and the results reported herein were for spectra that had reached equilibrium (no changes was observed with time). The high-temperature limit is set to 82 °C for all measurements to avoid the boiling point of DME (~85 °C) and possible melting of adduct material. ^{1}H and ^{19}F spin−lattice relaxation time (T_1) measurements utilized the inversion-recovery (180° − τ_{delay} − 90°—acquisition) method, and spin−spin relaxation times (T_2) were measured using the Carr−Purcell−Meiboom−Gill (CPMG) method (90° − τ_{delay} − [180° − τ_{delay}]$_n$—

https://dx.doi.org/10.1021/acs.jpcc.9b10212
J. Phys. Chem. C 2020, 124, 4999−5008

acquisition) with a delay time τ_{delay} = 83.33 μs (=2/24 kHz), which was synchronized to the spinning speed of 24 kHz.

Two-dimensional ^{1}H and ^{19}F NMR. 2D ^{19}F−^{19}F EXSY (NOESY) experiments were carried out using the "noesyph" pulse sequence included with Bruker's Topspin software with spectral width = 10 ppm (5647 Hz), number of increments = 128, number of scans = 8, and several mixing times (5, 10, 30, 50, 100, 300, and 500 ms) at 8 and 20 °C but only two mixing times (30 and 50 ms) at other temperatures. 2D ROESY experiments used the pulse sequence "roesyph.2" in Topspin software with the same parameters as those used for the NOESY experiment except that the number of scans was increased to 128 or 256 due to the lower sensitivity of the experiment and the carrier frequency (o1p) was shifted 15 ppm downfield to minimize the TOCSY artifacts. 2D ^{1}H−^{1}H EXSY utilized similar parameters to the ^{19}F experiments but with only one mixing time of 200 ms.

Exchange Rate Constant Calculation from 2D EXSY. Due to the inherently much lower sensitivity in ROESY (via spin−spin relaxation) than NOESY (via spin−lattice relaxation), we calculated exchange rates using NOESY after first confirming that the cross peaks observed were indeed from chemical exchange and not the result of dipolar cross-relaxation via ROESY. In a 2D EXSY spectrum, the 2D peak volume at row i and column j at a mixing time of t_m can be expressed as[28,29]

$$I_{ij}(t_m) = (e^{-\mathbf{R}t_m})_{ij} M_j^0$$

Here, M_j^0 is the magnetization of the nuclei at site j at equilibrium and $\mathbf{R}$ is the rate-constant matrix with the values $\mathbf{R}_{ij} = -k_{ji}$, the first-order exchange rate constant from site j to site i. Therefore, the rate-constant matrix can be calculated directly from the peak-volume matrix $\mathbf{A}$, with $\mathbf{A}_{ij} = I_{ij}(t_m)/M_j^0$

$$\mathbf{R} = -\frac{1}{t_m}\ln(\mathbf{A}) = -\frac{1}{t_m}\mathbf{U}\ln(\lambda)\mathbf{U}^{-1}$$

Here, $\mathbf{U}$ and λ are the eigenvectors and eigenvalues of $\mathbf{A}$.

In our case of four-site mutual exchange, with $M_1^0 = M_2^0 = M_3^0 = M_4^0$, we adopted a common treatment[30] to average out the experimental error by replacing the cross peak volumes I_{ij} and I_{ji} by their average value $(I_{ij} + I_{ji})/2$. The rate constants were calculated at each mixing time, and the average value is reported.

The exchange rate constant, k, was obtained from 2D EXSY according to the Eyring formulation[31,32]

$$\ln\left(\frac{k}{T}\right) = \ln\left(\frac{k_B}{h}\right) - \frac{\Delta H^{\neq}}{RT} + \frac{\Delta S^{\neq}}{R}$$

The enthalpy ($\Delta H^{\neq}$) and the entropy ($\Delta S^{\neq}$) of activation can be calculated from the slope and intercept of the Eyring plot of $\ln(k/T)$ vs $\ln(k_{B/h})$. Since we only have four reliable data points of rate constants vs temperature, an unacceptable error may be associated with the intercept of the plot, so we only report $\Delta H^{\neq}$ in Table 1.

Computational Methods. DFT calculations were conducted with the Amsterdam Density Functional (ADF) software.[33−35] Initial cluster model geometries were obtained from previously reported crystal structures[9] and optimized using the generalized gradient approximation with Grimme's third-generation dispersion corrections with moderate BJ dampening applied to the Perdew−Burke−Ernzerhof functional [GGA: PBE-D3(BJ)].[36,37] A Slater-type, all-electron, triple ζ, two-polarization function (TZ2P) was used as the basis set.[38] The numerical quality was set to Becke Excellent. NMR shielding tensors were calculated as implemented in ADF.[39−41] We employed 2,2,2-trifluoroethanol and trifluoroacetic acid as computational reference compounds with their experimental ^{19}F chemical shift at −77.8 and −76.55 ppm, respectively. The corresponding calculated ^{19}F chemical shifts in these compounds are −78.4 and −76.6 ppm; in reasonable agreement with the experimental observations.

RESULTS AND DISCUSSION

TFSI Conformational Fingerprints Using ^{19}F NMR Chemical Shift. We began with three solid-state salts, LiTFSI, NaTFSI, and Mg(TFSI)$_2$, as their crystal structures with detailed TFSI conformal states were reported previously.[16,17,19,42] As shown in Figure 1, clear differences in the

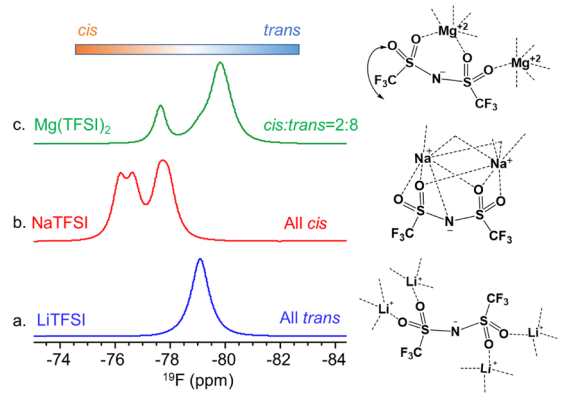

Figure 1. ^{19}F MAS spectra of LiTFSI (blue), NaTFSI (red), and Mg(TFSI)$_2$ (green) collected at 20 °C with a spinning speed of 32 kHz.

chemical shift of the ^{19}F MAS NMR spectra are observed by changing cations, indicating the presence of different TFSI conformational states due to the different cation sizes and ionic strengths of the counter cation. For example, in anhydrous LiTFSI salt,[17,42] Li^+ is coordinated tetrahedrally to sulfonyl oxygen atoms from four different neighboring TFSI anions in trans conformational arrangements (see Figure 1a). This structural arrangement yields a nearly identical local environment at the terminal CF_3 groups, thus giving rise to a sharp resonance at −79.1 ppm with a linewidth of 430 Hz. In the anhydrous NaTFSI salt,[19] the crystal structure has two ion pairs with two distinct Na^+ and TFSI in an asymmetric unit, in which both Na^+ cations have five primary coordinating oxygen atoms and two secondary coordinating atoms (one oxygen and one nitrogen), and both TFSI adopt a cis conformation. ^{19}F NMR of the NaTFSI salt (Figure 1b) shows three resonance at −76.21, −76.66, and −77.75 ppm, with the integrated ratios of 1:1:2, suggesting that the four CF_3 groups of the two TFSI experience slightly different local environments. Moving a step further from alkali to alkaline cation in anhydrous Mg(TFSI)$_2$,[16] Mg^{2+} engages in an octahedral manner to four TFSI with two TFSI providing two oxygen each and another two TFSI providing one oxygen each, so each TFSI in turn contacts two Mg^{2+} with two oxygen from two different sulfur binding to one Mg^{2+} and another oxygen binding to the second Mg^{2+}. The uncoordinated oxygen in TFSI provides enough conformational freedom to adopt either the cis or trans isomer at the same positions within the crystal structure. Evidently,

https://dx.doi.org/10.1021/acs.jpcc.9b10212
J. Phys. Chem. C 2020, 124, 4999−5008

the $Mg(TFSI)_2$ crystal has 18% of cis and 82% of trans TFSI conformational arrangements, which is reflected as three ^{19}F MAS NMR resonances at −77.68, −78.98, and −79.84 ppm, with the integration ratio of 20:5:75 (see Figure 1c). The ^{19}F NMR chemical shift trends among these TFSI-based salts reveal that the cis configuration exhibits downfield-shifted signals relative to the trans configuration. Although the local bonding environment can also dictate chemical shift, the general trend established for cis and trans configurations serves as an aid in the analysis of the conformational structure of TFSI in different materials. Nevertheless, the local dynamics and associated conformational flexibility in these salt samples were not discernable by NMR owing to the much slower timescale of these processes resulting from stronger electrostatic interactions within these more rigid crystal structures.

Unlike the alkali and alkaline earth based TFSI salts, the DME-based adduct structure ($Mg(TFSI)_2$·DME) may offer enhanced conformational flexibility due to solvent molecules screening the electrostatic interaction between anions and cations. The crystal structure of this adduct material, reported by Salama et al.,[9] showed that Mg^{2+} octahedrally coordinates with three DME molecules in a bidentate formation whereas the TFSI anions are uncoordinated and approximately 4.5 Å away from Mg^{2+} with highly disordered positions. This unique configuration could allow greater conformational flexibility for the TFSI molecules and offer an opportunity to establish a spectroscopic finger print and evaluation of the dynamics through consideration of chemical shift values, linewidth variations (motional narrowing), as well as 2D exchange experiments.

Figure 2 shows the ^{19}F MAS NMR spectrum of $Mg(TFSI)_2$·DME obtained at a spinning of 24 kHz with a sample

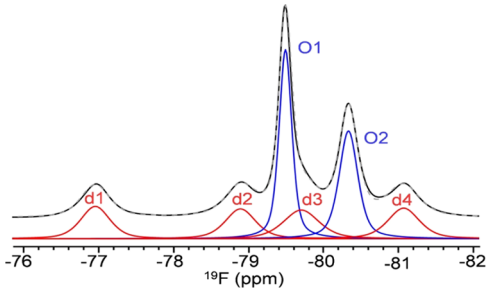

Figure 2. ^{19}F MAS spectrum of $Mg(TFSI)_2$·DME collected at 8 °C with a spinning speed of 24 kHz. The black line is the experimental spectrum, red and blue lines represent the two sets of deconvolution peaks with the fractions $f_{d1} = f_{d2} = f_{d3} = f_{d4}$ and $f_{O1} = f_{O2}$. The gray dash line is the sum of all deconvolution peaks.

temperature of 8 °C. Deconvolution of the spectrum reveals six distinct resonances that can be grouped into two sets on the basis of the intensity and linewidth. The first set of resonances (represented by red lines) has four peaks centered at −76.96 (d1), −78.90 (d2), −79.70 (d3), and −81.10 ppm (d4), with identical intensity and linewidth (260 Hz). The next set constitutes two higher-intensity peaks located at −79.49 ppm (O1) and −80.35 ppm (O2) with equal integrated area, albeit O1 has a relatively narrower linewidth (108 Hz) than O2 (170 Hz). To correlate these peaks to respective sites of TFSI molecules within the adduct crystal structure, we performed two-dimensional (2D) $^{19}F-^{19}F$ NOESY and ROESY NMR measurements.

Figure 3a shows the $^{19}F-^{19}F$ 2D NOESY spectrum of $Mg(TFSI)_2$·DME measured at room temperature. The

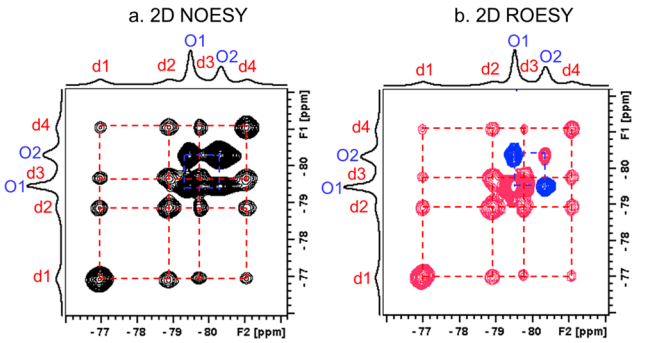

Figure 3. $^{19}F-^{19}F$ 2D NOESY (a) and ROESY (b) spectra of $Mg(TFSI)_2$·DME obtained at 8 °C with a spinning speed of 24 kHz and a mixing time of 30 ms. The experimental time for NOESY and ROESY measurements is 1.5 and 13.5 h, respectively. In the 2D ROESY plot, the negative cross peaks (between O1 and O2) are denoted with blue contours while the positive cross peaks (between d1, d2, d3, and d4) appear as red contours.

NOESY correlation spectrum displays positive pure-phase cross peaks for both the first (d1, d2, d3, d4) and second (O1and O2) set of resonances. These cross peaks could represent either dipolar coupling (due to closer proximity) or chemical exchanges between adjacent sites. To delineate between these two probable mechanisms, we performed $^{19}F-^{19}F$ 2D ROESY measurements. In ROESY spectra, the cross peaks will register a negative intensity (opposite phase of the diagonal) if the underlying mechanism is the dipolar cross-relaxation through space. Figure 3b shows the 2D ROESY spectrum where the cross peaks are positive for the first set of resonances (d1, d2, d3, and d4) and negative for the second set (O1 and O2). This indicates that the first set of four resonances (d1, d2, d3, and d4) are in chemical exchange with each other with distinguishable exchange rates, while the second set of resonances (O1 and O2) are being affected by dipolar coupling correlated through spin diffusion across closer proximity in space (typically <5 Å). Note that although intra- and intermolecular F−F distances are usually >4 Å in $Mg(TFSI)_2$·DME crystal structures,[9] the significant negative cross peak in ROESY may be the result from the strong spin diffusion effect, especially considering the bath of fluorine in the layered hydrophobic fluorous domain, as reported in crystal structures of many TFSI-containing salts.[16−19,43]

A reasonable model to explain these 1D and 2D NMR results together with previously reported single-crystal structural data[9] is to categorize TFSI sites into two regimes, namely, crystalline and disordered. In the crystalline region, TFSI anions reside in the second coordinating shell of Mg^{2+}, whereas in disordered regions, TFSI reside in third or fourth coordinating layers of Mg^{2+} that surround the crystalline region. A schematic illustration of these crystalline and disordered regions is shown in Scheme 2. The crystalline region has a hydrophobic fluorous layer where CF_3 groups of adjacent TFSI molecules are packed closely, leading to a dipolar coupled spin diffusion process, as indicated by the negative cross peaks in the ROESY spectra. Hence, we assign the resonances O1 and O2, with equal integration areas, to the two CF_3 groups of one TFSI molecule within the hydrophobic fluorous layers of the crystalline region. The slightly larger

https://dx.doi.org/10.1021/acs.jpcc.9b10212
J. Phys. Chem. C 2020, 124, 4999−5008

Scheme 2. Schematic Diagram of the Two Types of TFSI Anions in $Mg(TFSI)_2$·DME[a]

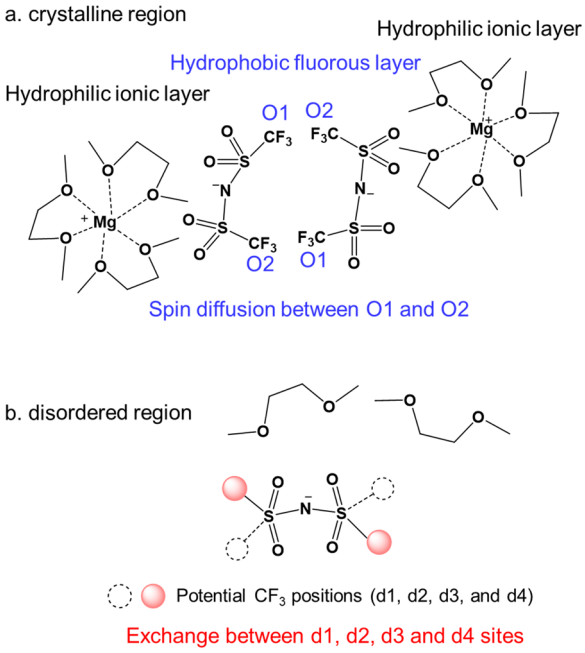

[a](a) Resonances O1 and O2 correlate to each other through spin diffusion in the hydrophobic fluorous layer of the crystalline region, and (b) resonances d1, d2, d3, and d4 exchange with each other by flipping of CF3 group or rotation of the entire TFSI in the disordered region.

linewidth of peak O2 may be explained by dampened dynamics of this CF_3 by its relatively closer proximity to $[Mg(DME)_3]^{2+}$ than the CF_3 of peak O1. On the other hand, the TFSI molecules in the disordered region reside further from Mg^{2+} and hence have greater conformational flexibility leading to CF_3 group exchange between different sites. Evidently, the four resonances with identical peak heights and widths, d1, d2, d3, and d4, correspond to the four sites that the two CF_3 groups of a single TFSI molecule can occupy within the disordered region (Scheme 2b). The formation of the disordered region may be the result of (1) weak coordinating power of TFSI anions due to their conformational flexibility and highly delocalized charge, (2) weakened coordinating power of $[Mg(DME)_3]^{2+}$ compared to Mg^{2+}, and (3) presence of remnant solvent DME from nucleation residing in the disordered region. The ^{1}H NMR spectrum (Figure S3) confirms the presence of crystalline DME (well-defined ^{1}H peaks at 4.20 and 3.90 ppm) and remnant DME (a broad peak between 0 and 10 ppm). A certain amount of physically adsorbed DME may be left in the material during the drying process to produce crystals of $Mg(TFSI)_2$·DME. The supersaturated solution (3.65 g $Mg(TFSI)_2$ dissolved in 4.5 g DME) used to precipitate the crystal has a DME to Mg^{2+} ratio of 8, while DME to Mg^{2+} ratio is 3 for the crystalline region detected by SCXRD,[9] we have approximately two DME left in the disordered region, estimated from ^{1}H NMR (Figure S3) and mass loss measurement. The fraction $f_{d1+d2+d3+d4}/f_{O1+O2}$ = 0.55:0.45 indicates that slightly more TFSI stays in the disordered region than the ordered region, which explains why SCXRD cannot accurately map TFSI positions. TFSI anions in these two regions may exhibit similar properties as the solvent-separated ion pairs present in electrolytes and electrolyte−electrode interphases that play a key role in battery performance.

To further evaluate our model of correlating NMR resonances to TFSI conformational arrangements, we performed DFT based ^{19}F chemical shift calculations. We begin with an isolated TFSI anion, where the trans configuration yields a single chemical shift value of −80.8 ppm whereas the cis configuration yields two distinct chemical shifts (−78.3 and −81.3 ppm) for the two CF_3 groups. This is consistent with our previous observation (see Figure 1a) that the cis conformer appears downfield (by a few ppm) from the trans conformer. With this theoretically validated chemical shift trend, we performed large cluster DFT calculations of

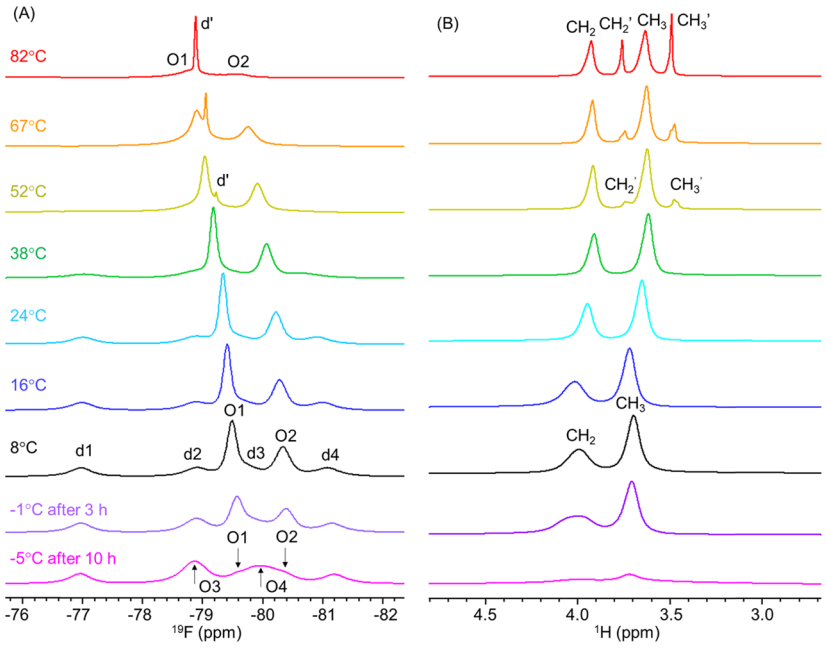

Figure 4. ^{19}F and ^{1}H MAS spectra of $Mg(TFSI)_2$·DME from −5 to 82 °C acquired at equilibrium, with a spinning speed of 24 kHz.

https://dx.doi.org/10.1021/acs.jpcc.9b10212
J. Phys. Chem. C 2020, 124, 4999−5008

$Mg(DME)_3(TFSI)_2(DME)_n$ structures, which represents the disordered region. The choice of this cluster is based on a previously reported single-crystal structure of the adduct material.[9] As shown in Figure S7, ^{19}F chemical shifts of TFSI in the clusters are located between 76.6 and 81.0 ppm for clusters with n varying from 0 to 4. The significant variation in the calculated chemical shift with the number of DME molecules in the secondary solvation shell is not surprising considering the oversimplification of a periodic crystalline structure to definitive molecular cluster models employed in our DFT calculations. Nevertheless, the span of calculated chemical shifts (~4.4 ppm) of the clusters is consistent with the experimental value (81.10−76.96 = 4.14 ppm, as shown in Figure 2) so it is reasonable to assume that the d1 to d4 sites are from TFSI located in the disordered region, which resembles the $Mg(DME)_3(TFSI)_2(DME)_n$ clusters.

TFSI Conformational and Dynamic Changes. Armed with spectroscopic signatures of different TFSI conformational structures within the adduct structure, we can now analyze the site-specific dynamics using variable temperature (from −5 to 82 °C) 1D and 2D NMR. A set of variable temperature 1D ^1H and ^{19}F NMR spectra are presented in Figure 4. As the temperature increases, ^{19}F NMR reveals that the four resonances representing CF_3 sites within the disordered region (d1, d2, d3, and d4) undergo a coalescence process indicating thermally activated chemical exchange. At higher temperature (~52 °C), all four resonances coalesced to a broad resonance between −77 and −81 ppm and a small sharp resonance (d′) shifted toward a high field (−79.25 ppm). The deconvolution analysis of this coalescence process is shown in the Supporting Information (Figure S4). Similar to the observation in solid-state lithium-ion conductors,[44] this composite of a narrow and a broad component in the NMR peak is caused by a distribution of CF_3 (TFSI) motions: the narrow component is from CF_3 with faster molecular motion, whereas the broad component is from CF_3 with slower motion. As the temperature increases further, the intensity of this sharp peak (d′) representing the disordered region increases at the cost of the broad peak as well as the broadening of resonances O1 and O2 from the ordered region. Meanwhile, ^1H NMR at a high temperature (≥52 °C) also shows a new set of peaks located at 3.98 and 3.71 ppm, which are upfield-shifted from the original peaks of solvate DME coordinated with Mg^{2+} (i.e., $[Mg(DME)_3]^{2+}$). To further analyze these new peaks observed at higher temperatures, we performed $^{19}F-^{19}F$ and $^1H-^1H$ 2D NOESY measurements. The $^{19}F-^{19}F$ NOESY spectrum (see Figure 5a) indicates that the coalesced peak d′ representing the disordered region does not correlate or exchange with O1 and O2 peaks of the ordered region. Similarly, the $^1H-^1H$ NOESY spectrum (see Figure 5b) shows that the two new peaks are correlated with each other, suggesting that these two new ^1H signals are from DME molecules with slightly different chemical environments than the solvated DME. It should be noted that the ^1H NMR chemical shifts of neat DME are observed at 3.54 and 3.37 ppm so the observed new peaks were potentially representing a new coordinating environment rather than representing "free" DME molecules. Additionally, the increase of the new ^1H peaks is accompanied by the decrease of the signals from solvate DME, further suggesting structural evolution of solvated DME within the adduct structure. With the above combined information, we propose that when $T \geq 52$ °C, some of the solvated DME molecules gain enough thermal energy to escape the first coordinating

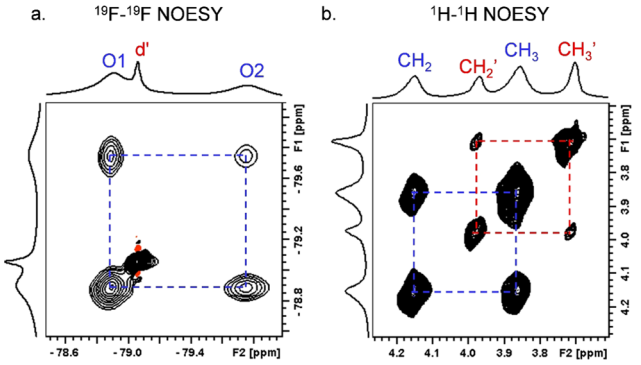

Figure 5. $^{19}F-^{19}F$ 2D NOESY (left) and $^1H-^1H$ 2D NOESY (right) spectra of $Mg(TFSI)_2$·DME obtained at 67°C with a spinning speed of 24 kHz and a mixing time of 30 ms for $^{19}F-^{19}F$ NOESY and 200 ms for $^1H-^1H$ NOESY.

shell. This facilitates faster tumbling of TFSI in the disordered region, thus increasing the rate of chemical exchange between d1, d2, d3, and d4, yielding the coalesced new sharp peak d′. In contrast, resonances O1 and O2 grow slightly narrower between 8 and 38 °C due to the increase of molecular motion of TFSI within the crystalline region. But the linewidths of O1 and O2 appear to be broadened at $T \geq 52$ °C, probably due to the potential exchange that begins to happen between the two sites when the "escaping" solvate DME interacts with TFSI of the crystalline region. At 82 °C, the resonances O1 and O2 became closer to each other with significant line broadening due to further increase of the TFSI mobility, as observed from the coalescing process of d1, d2, d3, and d4. A further increase in temperature may eventually access a state where molecular motion of all TFSI is on the NMR timescale, leading to an exchange-averaged single peak representing both the ordered and disordered regions that is similar to results from TFSI-containing solutions.

In the low-temperature regime (≤8 °C), the ^{19}F NMR linewidth of resonances O1 and O2, representing TFSI molecules from the crystalline region, increases, as evidenced by loss of signal height shown in Figure 4 (more detailed thermal and data analysis are reported in the Supporting Information Figure S5). This line broadening leads to considerable signal overlap with d2 and d3 resonances. The peak deconvolution analysis based on a Gaussian/Lorentizan fitting method reveals the presence of new peaks (labeled as O3 and O4 in Figure 4) within this overlapped region. To validate the presence of these new peaks and to correlate with specific CF_3 sites within the adduct structure, we performed $^{19}F-^{19}F$ 2D NOESY experiments. The NOESY spectra measured at −5 °C (see Figure 6), confirms the evolution of new resonances O3 and O4 located at −78.87 and −79.93 ppm, which are 0.72 and 0.48 ppm downfield-shifted from O1 and O2 resonances of the crystalline region, respectively. Similar to O1 and O2, O3 and O4 correlate with each other but not with any other peaks. Hence, on the basis of their chemical shift trend and dipolar relaxation-induced cross peaks, we propose that O3 and O4 result from the two CF_3 of the same TFSI with cis form at the second coordinating shell of the crystalline region, while O1 and O2 are from TFSI adopting the trans form. Similarly, the ^1H NMR also shows a dramatic increase in linewidth of both CH_2 and CH_3 peaks with decreases in intensity, indicating that the conformational change of second-shell coordinating TFSI are correlated with

https://dx.doi.org/10.1021/acs.jpcc.9b10212
J. Phys. Chem. C 2020, 124, 4999−5008

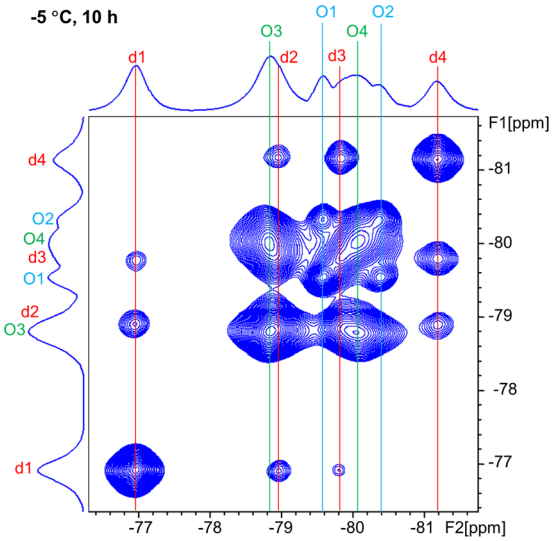

Figure 6. $^{19}F-^{19}F$ 2D NOESY spectrum of freshly prepared $Mg(TFSI)_2$·DME obtained at −5 °C and equilibrated for 10 h. The MAS spinning speed is 24 kHz and the mixing time is 30 ms.

the dampened motion of coordinated DME within the crystalline region. It is intriguing to note the arising of new O3 and O4 peaks along with severely dampened DME dynamics at lower temperatures (≤−5 °C). Typically, at lower temperatures, restricted molecular motions would indicate preference for a more rigid crystal structure with higher coordinating power. For TFSI molecules, the relatively higher-coordinating cis conformer is preferred at lower temperature due to its greater dipole moment than the trans conformer (μ = 5.42 D in cis vs 0.67 D in trans).[12] With increasing temperature, enhanced molecular motion of DME and TFSI favors a less rigid structure, therefore the trans conformer is preferred with only one side of O═S═O coordinating to $[Mg(DME)_3]^{2+}$ and the other side remaining more flexible. This conversion of trans to cis is a slow process with a reaction rate of ~2×10^{-5} s^{-1} calculated from the change of ^{19}F NMR spectra with time at −5 °C (spectra and data analysis are shown in Figure S5).

Thermodynamics and Kinetics of TFSI Conformational Flexibility. Since NMR detects site-specific molecular motion directly, we can monitor the temperature-dependent chemical and conformational exchange process within this complex adduct structure. As a first step, we calculated the exchange rate constants in the low-temperature region (from 16 to −5 °C) between four sites d1, d2, d3, and d4 from 2D exchange spectroscopy (EXSY) (see the Experimental Methods section for details). Although all exchanges between d1, d2, d3, and d4 are mutual, the rate constants are significantly different, as shown in Table 1. When $T \leq 8$ °C, the general trend is that $k_{d1\rightleftharpoons d2} > k_{d1\rightleftharpoons d3} > k_{d1\rightleftharpoons d4}$, $k_{d3\rightleftharpoons d4} > k_{d2\rightleftharpoons d4} > k_{d2\rightleftharpoons d3}$. The fastest exchanges d1 ⇌ d2 and d3 ⇌ d4 may correspond to the flip of a CF_3 group around the S−C bond; therefore, d1 and d2 are attributed to the two sites that can be occupied by one CF_3 group of TFSI in the disordered region, and d3 and d4, to the other CF_3 group of the same TFSI (see Scheme 3). The slowest exchange d1 ⇌ d4 happens between the two sites with largest chemical shift difference (4.14 ppm at 8 °C), indicating the exchange reflects the greatest change in the local chemical environment; hence we assign d1 and d4 to the opposite sides of S−N−S, and d1 ⇌ d4 can only be realized by rotation of the entire TFSI anion by 180°. The potential chemical exchange processes between the four sites are summarized in Scheme 3: (1) rotation of S−C bond − flipping of CF_3 group (d1 ⇌ d2, d3 ⇌ d4), (2) rotation of S−N−S bond along the z-axis that is within the S−N−S plane (d1 ⇌ d3 and d2 ⇌ d4), and (3) rotation of S−N−S bond along the y-axis that is normal to the plane (d1 ⇌ d4 and d2 ⇌ d3).

Scheme 3. Potential Conformational Exchange Routes of TFSI in the Disordered Region

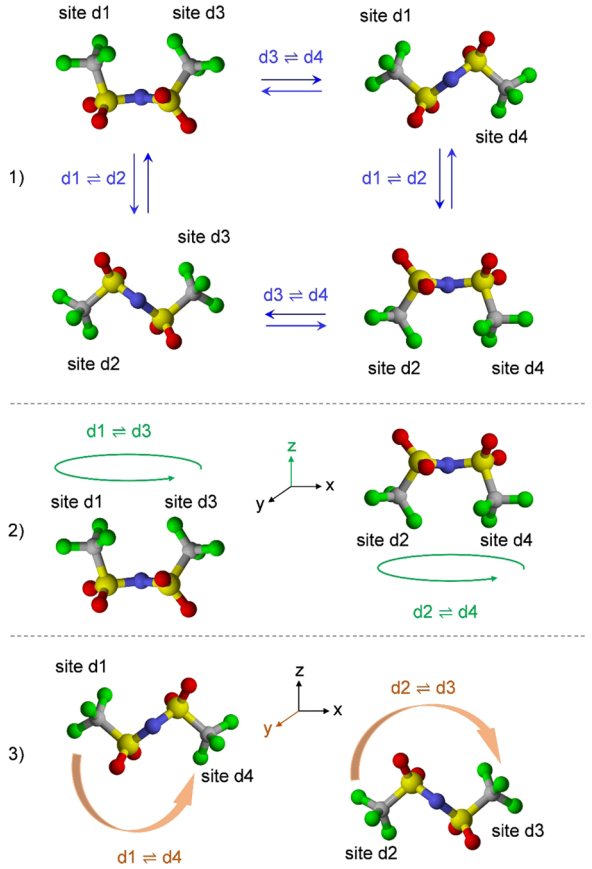

Table 1. Mutual Exchange Rate Constants of d1 ⇌ d2, d1 ⇌ d3, d1 ⇌ d4, d2 ⇌ d3, d2 ⇌ d4, and d3 ⇌ d4 Calculated from 2D EXSY, and Activation Enthalpy $\Delta H^{\neq}$ Estimated Using Eyring Plot

T (°C)/k (s^{-1})	$k_{d1\rightleftharpoons d2}$	$k_{d1\rightleftharpoons d3}$	$k_{d1\rightleftharpoons d4}$	$k_{d2\rightleftharpoons d3}$	$k_{d2\rightleftharpoons d4}$	$k_{d3\rightleftharpoons d4}$
−5	7.6	3.1	0.7	6.4	7.8	10.4
1	10.4	4.5	2.0	8.4	11.5	13.0
8	13.6	5.6	4.8	9.5	12.1	17.6
16	16	7.5	19.2	15.0	17.8	19.7
$\Delta H^{\neq}$ (kJ/mol)	21 ± 3	24 ± 3	98 ± 10	23 ± 3	21 ± 3	19 ± 3

https://dx.doi.org/10.1021/acs.jpcc.9b10212
J. Phys. Chem. C 2020, 124, 4999−5008

Despite significantly different exchange rates, the activation enthalpy for TFSI conformational flexibility within the disordered region is comparable for d1 ⇌ d2, d1 ⇌ d3, d2 ⇌ d3, d2 ⇌ d4, and d3 ⇌ d4. For example, the highest activation enthalpy of $\Delta H^{\neq}_{d1\rightleftharpoons d3}$ = 24 ± 3 kJ/mol and lowest enthalpy of $\Delta H^{\neq}_{d3\rightleftharpoons d4}$ = 19 ± 3 kJ/mol are observed for TFSI conformal exchange processes, suggesting that the transition between trans and cis conformers through flipping of a CF_3 group around a S−C bond requires an activation energy of ∼20 kJ/mol in the low-temperature regime. The exchange between d1 and d4 is the slowest at $T \leq 8$ °C but becomes fastest when $T \geq 16$ °C, yielding a dramatically greater activation energy $\Delta H^{\neq}_{d1\rightleftharpoons d4}$ = 98 ± 10 kJ/mol compared with other exchanges. This may be explained by the fact that this exchange demands the rotation of the entire TFSI and the interactions (electrostatic, dipolar, and van der Waals) between TFSI and its local environment, including DME, other TFSI, and $Mg(DME_3)^{2+}$, are particularly not favorable for this exchange.

To further evaluate the energy requirements for the cis to trans conformational transition process for the TFSI anion, we calculated the activation energy by performing a pseudorotation of TFSI with the dihedral angle ϕ(S−N−S−C) varying from −90 to 90°, as shown in Figure 7. The activation energy

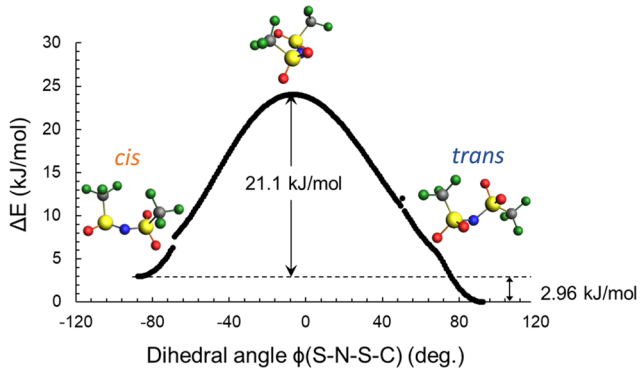

Figure 7. Potential energy curve for the pseudorotation of TFSI by varying ϕ(S−N−S−C) from −90 to 90°.

ΔE_a = 21.1 kJ/mol derived from the potential energy curve dihedral angle rotation matches well with our experimentally measured enthalpy of 19−21 kJ/mol. It should be noted that entropic considerations account for less than 2% of the calculated barrier.

CONCLUSIONS

In the work presented here, we detected distinct TFSI conformal states and associated exchange rates as well as activation energies within the adduct material $Mg(TFSI)_2$·DME using ^{19}F 1D and 2D solid-state MAS NMR. The combination of ^{19}F single-pulse, 2D NOESY, and ROESY NMR experiments demonstrates that at 8 °C, 45% of adduct TFSI stays in the crystalline region adopting the trans conformer, while 55% of the TFSI remains in the disordered region where TFSI experiences conformational exchange between cis and trans conformations. The cis−trans exchange rate is estimated to be 13.6−17.6 s^{-1} at 8 °C with $\Delta H^{\neq}$ = 19−24 kJ/mol, but the rotation of the entire TFSI anion is slower at a rate of 4.8 s^{-1} at 8 °C with a significantly greater $\Delta H^{\neq}$ = 98 ± 10 kJ/mol. As the temperature increases, the exchange rates become faster in the disordered region and then in the crystalline area. Concurrently, ^{1}H NMR shows that some coordinating DME molecules (with Mg^{2+}) disengage from the first coordinating shell at $T \geq 52$ °C. On the other hand, as temperature decreases to $T \leq -1$ °C, TFSI within the crystalline region slowly undergoes conformational change from trans to cis at a conversion rate of 1.9×10^{-5} s^{-1} because the significantly reduced molecular motion of TFSI and DME at a lower temperature prefers the cis conformer with a greater dipole moment. Furthermore, DFT calculations provide ^{19}F chemical shift values that are consistent with our assignment for cis/trans conformers, and the activation energy value for cis−trans transition (21.1 kJ/mol) is also in good agreement with our experimental result. The combination of ^{19}F and ^{1}H 1D and 2D NMR experiments with DFT NMR calculations demonstrated here will be further used to study TFSI conformation, dynamics, and decomposition products within electrode−electrolyte interphases where TFSI molecular motion may lie at the similar timescale as in the adduct material. Such studies are critical for detailing the structural and dynamic requirements for enhanced Mg transport across the complex networks formed on electrodes, which will depend strongly on the types and distributions of heterogeneous phases formed within the interphase.

ASSOCIATED CONTENT

Supporting Information

The Supporting Information is available free of charge at https://pubs.acs.org/doi/10.1021/acs.jpcc.9b10212.

Temperature calibration for fast magic angle spinning; ^{19}F−^{19}F 2D NOESY and ROESY spectra of $Mg(TFSI)_2$ at 8 °C; deconvolution of ^{1}H MAS NMR spectrum of $Mg(TFSI)_2$·DME at 8 °C; deconvolution of ^{19}F MAS NMR spectrum of $Mg(TFSI)_2$·DME at 67 °C; conversion of trans to cis TFSI conformers in the crystalline region at −5 °C demonstrated by time-dependent ^{19}F 1D NMR and 2D NOESY spectra; comparison of ^{19}F and ^{1}H MAS spectra of $Mg(TFSI)_2$·DME before heating and after cooling down from 82 °C; ^{19}F chemical shift values of $Mg(TFSI)_2$·DME clusters calculated using TZ2PJ basis set using ADF2018 package (PDF)

AUTHOR INFORMATION

Corresponding Authors

Karl T. Mueller − *Pacific Northwest National Laboratory (PNNL), Richland, Washington 99352, United States; The Joint Center for Energy Storage Research (JCESR), Lemont, Illinois 60439, United States;* orcid.org/0000-0001-9609-9516; Phone: (509) 371-6550; Email: Karl.Mueller@pnnl.gov

Vijayakumar Murugesan − *Pacific Northwest National Laboratory (PNNL), Richland, Washington 99352, United States; The Joint Center for Energy Storage Research (JCESR), Lemont, Illinois 60439, United States;* orcid.org/0000-0001-6149-1702; Phone: (509) 371-6540; Email: Vijay@pnnl.gov

Authors

Ying Chen − *Pacific Northwest National Laboratory (PNNL), Richland, Washington 99352, United States; The Joint Center for Energy Storage Research (JCESR), Lemont, Illinois 60439, United States;* orcid.org/0000-0001-7417-0991

https://dx.doi.org/10.1021/acs.jpcc.9b10212
J. Phys. Chem. C 2020, 124, 4999−5008

Nicholas R. Jaegers − *Pacific Northwest National Laboratory (PNNL), Richland, Washington 99352, United States;* orcid.org/0000-0002-9930-7672

Kee Sung Han − *Pacific Northwest National Laboratory (PNNL), Richland, Washington 99352, United States; The Joint Center for Energy Storage Research (JCESR), Lemont, Illinois 60439, United States;* orcid.org/0000-0002-3535-1818

Hui Wang − *Pacific Northwest National Laboratory (PNNL), Richland, Washington 99352, United States; The Joint Center for Energy Storage Research (JCESR), Lemont, Illinois 60439, United States*

Robert P. Young − *Pacific Northwest National Laboratory (PNNL), Richland, Washington 99352, United States*

Garvit Agarwal − *Argonne National Laboratory (ANL), Lemont, Illinois 60439, United States; The Joint Center for Energy Storage Research (JCESR), Lemont, Illinois 60439, United States*

Andrew S. Lipton − *Pacific Northwest National Laboratory (PNNL), Richland, Washington 99352, United States*

Rajeev S. Assary − *Argonne National Laboratory (ANL), Lemont, Illinois 60439, United States; The Joint Center for Energy Storage Research (JCESR), Lemont, Illinois 60439, United States;* orcid.org/0000-0002-9571-3307

Nancy M. Washton − *Pacific Northwest National Laboratory (PNNL), Richland, Washington 99352, United States*

Jian Zhi Hu − *Pacific Northwest National Laboratory (PNNL), Richland, Washington 99352, United States; The Joint Center for Energy Storage Research (JCESR), Lemont, Illinois 60439, United States;* orcid.org/0000-0001-8879-747X

Complete contact information is available at: https://pubs.acs.org/10.1021/acs.jpcc.9b10212

Notes

The authors declare no competing financial interest.

■ ACKNOWLEDGMENTS

This work was supported as part of the Joint Center for Energy Storage Research (JCESR), an Energy Innovation Hub funded by the U.S. Department of Energy (DOE), Office of Science, Basic Energy Sciences (BES). NMR and computational portion of the research were performed at Environmental and Molecular Sciences Laboratory (EMSL), a DOE-Office of Science user facility supported by the Biological and Environmental Research (BER). PNNL is a multiprogram national laboratory operated for the DOE by Battelle Memorial Institute under Contract DE-AC06-76RLO 1830.

■ REFERENCES

(1) Hallett, J. P.; Welton, T. Room-Temperature Ionic Liquids: Solvents for Synthesis and Catalysis. 2. *Chem. Rev.* **2011**, *111*, 3508−3576.

(2) Lewandowski, A.; Świderska-Mocek, A. Ionic Liquids as Electrolytes for Li-Ion Batteries—an Overview of Electrochemical Studies. *J. Power Sources* **2009**, *194*, 601−609.

(3) Best, A. S.; Bhatt, A. I.; Hollenkamp, A. F. Ionic Liquids with the Bis(Fluorosulfonyl)Imide Anion: Electrochemical Properties and Applications in Battery Technology. *J. Electrochem. Soc.* **2010**, *157*, A903−A911.

(4) Ha, S.-Y.; Lee, Y.-W.; Woo, S. W.; Koo, B.; Kim, J.-S.; Cho, J.; Lee, K. T.; Choi, N.-S. Magnesium(Ii) Bis(Trifluoromethane Sulfonyl) Imide-Based Electrolytes with Wide Electrochemical Windows for Rechargeable Magnesium Batteries. *ACS Appl. Mater. Interfaces* **2014**, *6*, 4063−4073.

(5) Canepa, P.; Sai Gautam, G.; Hannah, D. C.; Malik, R.; Liu, M.; Gallagher, K. G.; Persson, K. A.; Ceder, G. Odyssey of Multivalent Cathode Materials: Open Questions and Future Challenges. *Chem. Rev.* **2017**, *117*, 4287−4341.

(6) Lapidus, S. H.; Rajput, N. N.; Qu, X.; Chapman, K. W.; Persson, K. A.; Chupas, P. J. Solvation Structure and Energetics of Electrolytes for Multivalent Energy Storage. *Phys. Chem. Chem. Phys.* **2014**, *16*, 21941−21945.

(7) Johansson, P.; Gejji, S. P.; Tegenfeldt, J.; Lindgren, J. The Imide Ion: Potential Energy Surface and Geometries. *Electrochim. Acta* **1998**, *43*, 1375−1379.

(8) Watkins, T.; Buttry, D. A. Determination of Mg2+ Speciation in a Tfsi−-Based Ionic Liquid with and without Chelating Ethers Using Raman Spectroscopy. *J. Phys. Chem. B* **2015**, *119*, 7003−7014.

(9) Salama, M.; Shterenberg, I.; Gizbar, H.; Eliaz, N. N.; Kosa, M.; Keinan-Adamsky, K.; Afri, M.; Shimon, L. J. W.; Gottlieb, H. E.; Major, D. T.; et al. Unique Behavior of Dimethoxyethane (Dme)/Mg(N(So2cf3)2)2 Solutions. *J. Phys. Chem. C* **2016**, *120*, 19586−19594.

(10) Shterenberg, I.; Salama, M.; Yoo, H. D.; Gofer, Y.; Park, J.-B.; Sun, Y.-K.; Aurbach, D. Evaluation of (Cf3so2)2n− (Tfsi) Based Electrolyte Solutions for Mg Batteries. *J. Electrochem. Soc.* **2015**, *162*, A7118−A7128.

(11) Rajput, N. N.; Qu, X.; Sa, N.; Burrell, A. K.; Persson, K. A. The Coupling between Stability and Ion Pair Formation in Magnesium Electrolytes from First-Principles Quantum Mechanics and Classical Molecular Dynamics. *J. Am. Chem. Soc.* **2015**, *137*, 3411−3420.

(12) Herstedt, M.; Smirnov, M.; Johansson, P.; Chami, M.; Grondin, J.; Servant, L.; Lassègues, J. C. Spectroscopic Characterization of the Conformational States of the Bis(Trifluoromethanesulfonyl)Imide Anion (Tfsi−). *J. Raman Spectrosc* **2005**, *36*, 762−770.

(13) Fujii, K.; Fujimori, T.; Takamuku, T.; Kanzaki, R.; Umebayashi, Y.; Ishiguro, S.-i. Conformational Equilibrium of Bis-(Trifluoromethanesulfonyl) Imide Anion of a Room-Temperature Ionic Liquid: Raman Spectroscopic Study and Dft Calculations. *J. Phys. Chem. B* **2006**, *110*, 8179−8183.

(14) Duluard, S.; Grondin, J.; Bruneel, J.-L.; Pianet, I.; Grélard, A.; Campet, G.; Delville, M.-H.; Lassègues, J.-C. Lithium Solvation and Diffusion in the 1-Butyl-3-Methylimidazolium Bis-(Trifluoromethanesulfonyl)Imide Ionic Liquid. *J. Raman Spectrosc.* **2008**, *39*, 627−632.

(15) Lassègues, J.-C.; Grondin, J.; Aupetit, C.; Johansson, P. Spectroscopic Identification of the Lithium Ion Transporting Species in Litfsi-Doped Ionic Liquids. *J. Phys. Chem. A* **2009**, *113*, 305−314.

(16) Veryasov, G.; Harinaga, U.; Matsumoto, K.; Hagiwara, R. Crystallographic Insight into the Mg2+ Coordination Mode and N(So2cf3)2− Anion Conformation in Mg[N(So2cf3)2]2 and Its Adducts. *Eur. J. Inorg. Chem.* **2017**, *2017*, 1087−1099.

(17) Nowinski, J. L.; Lightfoot, P.; Bruce, P. G. Structure of Lin(Cf3so2)2, a Novel Salt for Electrochemistry. *J. Mater. Chem.* **1994**, *4*, 1579−1580.

(18) Xue, L.; Padgett, C. W.; DesMarteau, D. D.; Pennington, W. T. Synthesis and Structures of Alkali Metal Salts of Bis-[(Trifluoromethyl)Sulfonyl]Imide. *Solid State Sci.* **2002**, *4*, 1535−1545.

(19) Matsumoto, K.; Matsui, T.; Nohira, T.; Hagiwara, R. Crystal Structure of Na[N(So2cf3)2] and Coordination Environment of Alkali Metal Cation in the M[N(So2cf3)2] (M+=Li+, Na+, K+, and Cs+) Structures. *J. Fluorine Chem.* **2015**, *174*, 42−48.

(20) Salama, M.; Shterenberg, I.; Shimon, L. J. W.; Keinan-Adamsky, K.; Afri, M.; Gofer, Y.; Aurbach, D. Structural Analysis of Magnesium Chloride Complexes in Dimethoxyethane Solutions in the Context of Mg Batteries Research. *J. Phys. Chem. C* **2017**, *121*, 24909−24918.

(21) R, D. J. W. *Guide to Fluorine NMR for Organic Chemists*; John Wiley & Sons, Inc.: Hoboken, New Jersey, 2016.

(22) Hayamizu, K.; Tsuzuki, S.; Seki, S. Molecular Motions and Ion Diffusions of the Room-Temperature Ionic Liquid 1,2-Dimethyl-3-Propylimidazolium Bis(Trifluoromethylsulfonyl)Amide (Dmpimtfsa)

Studied by 1h, 13c, and 19f NMR. *J. Phys. Chem. A* **2008**, *112*, 12027−12036.
(23) Kunze, M.; Montanino, M.; Appetecchi, G. B.; Jeong, S.; Schönhoff, M.; Winter, M.; Passerini, S. Melting Behavior and Ionic Conductivity in Hydrophobic Ionic Liquids. *J. Phys. Chem. A* **2010**, *114*, 1776−1782.
(24) Hayamizu, K.; Tsuzuki, S.; Seki, S.; Umebayashi, Y. Multinuclear NMR Studies on Translational and Rotational Motion for Two Ionic Liquids Composed of BF4 Anion. *J. Phys. Chem. B* **2012**, *116*, 11284−11291.
(25) D'Agostino, C.; Mantle, M. D.; Mullan, C. L.; Hardacre, C.; Gladden, L. F. Diffusion, Ion Pairing and Aggregation in 1-Ethyl-3-Methylimidazolium-Based Ionic Liquids Studied by 1H and 19F PFG NMR: Effect of Temperature, Anion and Glucose Dissolution. *ChemPhysChem* **2018**, *19*, 1081−1088.
(26) Brus, J. Heating of Samples Induced by Fast Magic-Angle Spinning. *Solid State Nucl. Magn. Reson.* **2000**, *16*, 151−160.
(27) Guan, X.; Stark, R. E. A General Protocol for Temperature Calibration of Mas NMR Probes at Arbitrary Spinning Speeds. *Solid State Nucl. Magn. Reson.* **2010**, *38*, 74−76.
(28) Macura, S.; Ernst, R. R. Elucidation of Cross Relaxation in Liquids by Two-Dimensional N.M.R. Spectroscopy. *Mol. Phys.* **1980**, *41*, 95−117.
(29) Perrin, C. L.; Gipe, R. K. Multisite Kinetics by Quantitative Two-Dimensional NMR. *J. Am. Chem. Soc.* **1984**, *106*, 4036−4038.
(30) Willem, R. 2D NMR Applied to Dynamic Stereochemical Problems. *Prog. Nucl. Magn. Reson. Spectrosc.* **1988**, *20*, 1−94.
(31) Eyring, H. The Activated Complex in Chemical Reactions. *J. Chem. Phys.* **1935**, *3*, 107−115.
(32) Laidler, K. J.; King, M. C. Development of Transition-State Theory. *J. Phys. Chem. A* **1983**, *87*, 2657−2664.
(33) te Velde, G.; Bickelhaupt, F. M.; Baerends, E. J.; Fonseca Guerra, C.; van Gisbergen, S. J. A.; Snijders, J. G.; Ziegler, T. Chemistry with ADF. *J. Comput. Chem.* **2001**, *22*, 931−967.
(34) Fonseca Guerra, C.; Snijders, G. J.; te Velde, G.; Baerends, J. E. Towards an Order-N DFT Method. *Theor. Chem. Acc.* **1998**, *99*, 391−403.
(35) *ADF2014 Scm*; Vrije Universiteit: Amsterdam, The Netherlands. http://www.scm.com, 2014.
(36) Perdew, J. P.; Burke, K.; Ernzerhof, M. Generalized Gradient Approximation Made Simple. *Phys. Rev. Lett.* **1996**, *77*, 3865−3868.
(37) Grimme, S.; Ehrlich, S.; Goerigk, L. Effect of the Damping Function in Dispersion Corrected Density Functional Theory. *J. Comput. Chem.* **2011**, *32*, 1456−1465.
(38) Van Lenthe, E.; Baerends, E. J. Optimized Slater-Type Basis Sets for the Elements 1−118. *J. Comput. Chem.* **2003**, *24*, 1142−1156.
(39) Schreckenbach, G.; Ziegler, T. Calculation of NMR Shielding Tensors Using Gauge-Including Atomic Orbitals and Modern Density-Functional Theory. *J. Phys. Chem. B* **1995**, *99*, 606−611.
(40) Schreckenbach, G.; Ziegler, T. The Calculation of NMR Shielding Tensors Based on Density Functional Theory and the Frozen-Core Approximation. *Int. J. Quantum Chem.* **1996**, *60*, 753−766.
(41) Schreckenbach, G.; Ziegler, T. Calculation of NMR Shielding Tensors Based on Density Functional Theory and a Scalar Relativistic Pauli-Type Hamiltonian. The Application to Transition Metal Complexes. *Int. J. Quantum Chem.* **1997**, *61*, 899−918.
(42) Henderson, W. A.; Seo, D. M.; Zhou, Q.; Boyle, P. D.; Shin, J.-H.; De Long, H. C.; Trulove, P. C.; Passerini, S. An Alternative Ionic Conductivity Mechanism for Plastic Crystalline Salt−Lithium Salt Electrolyte Mixtures. *Adv. Energy Mater.* **2012**, *2*, 1343−1350.
(43) Xue, L.; DesMarteau, D. D.; Pennington, W. T. Synthesis and Structures of Alkaline Earth Metal Salts of Bis[(Trifluoromethyl)-Sulfonyl]Imide. *Solid State Sci.* **2005**, *7*, 311−318.
(44) Gupta, A.; Murugan, R.; Paranthaman, M. P.; Bi, Z.; Bridges, C. A.; Nakanishi, M.; Sokolov, A. P.; Han, K. S.; Hagaman, E. W.; Xie, H.; et al. Optimum Lithium-Ion Conductivity in Cubic Li7−Xla3hf2−Xtaxo12. *J. Power Sources* **2012**, *209*, 184−188.

https://dx.doi.org/10.1021/acs.jpcc.9b10212
J. Phys. Chem. C 2020, 124, 4999−5008